Title
Ventilation measurements using fast-helical free-breathing computed tomography.

Journal
Medical Physics, 48(10)

Authors
Low, Daniel
OConnell, Dylan
Lauria, Michael
et al.

Publication Date
2021-10-01

DOI
10.1002/mp.15173

Peer reviewed

HHS Public Access

Author manuscript

Med Phys. Author manuscript; available in PMC 2022 October 01.

Published in final edited form as:

Med Phys. 2021 October ; 48(10): 6094–6105. doi:10.1002/mp.15173.

Ventilation Measurements Using Fast-Helical Free-Breathing CT

Daniel A. Low[a,e], **Dylan O'Connell**[a], **Michael Lauria**[a], **Bradley Stiehl**[a], **Louise Naumann**[a], **Percy Lee**[b], **John Hegde**[a], **Igor Barjaktarevic**[c], **Jonathan Goldin**[d], **Anand Santhanam**[a]

[a]Department of Radiation Oncology, University of California Los Angeles, Los Angeles, California 90095

[b]Department of Radiation Oncology, The University of Texas M.D. Anderson Cancer Center, Houston Texas 77030

[c]Department of Medicine, University of California Los Angeles, Los Angeles, California 90095

[d]Department of Radiology, University of California Los Angeles, Los Angeles, California 90095

Abstract

Purpose: To examine the use of multiple fast-helical free breathing CT (FHFBCT) scans for ventilation measurement

Methods: Ten patients were scanned 25 times in alternating directions using a FHFBCT protocol. Simultaneously, an abdominal pneumatic bellows was used as a real-time breathing surrogate. Regions-of-interest (ROIs) were selected from the upper right lungs of each patient for analysis. The ROIs were first registered using a published registration technique (pTV). A subsequent followup registration employed an objective function with two terms, a ventilation-adjusted Hounsfield Unit difference and a conservation-of-mass term labeled Δ that denoted the difference between the deformation Jacobian and the tissue density ratio. The ventilations were calculated voxel-by-voxel as the slope of a first-order fit of the Jacobian as a function of the breathing amplitude.

Results: The ventilations of the 10 patients showed different patterns and magnitudes. The average ventilation calculated from the DVFs of the pTV and secondary registration were nearly identical, but the standard deviation of the voxel-to-voxel differences were approximately 0.1. The mean of the 90th percentile values of ΔΓ were reduced from 0.153 to 0.079 between the pTV and secondary registration, implying first that the secondary registration improved the conservation-of-mass criterion by almost 50% and that on average the correspondence between the Jacobian and density ratios as demonstrated by ΔΓ were less than 0.1. This improvement occurred in spite of the average of the 90th percentile changes in the DVF magnitudes being only 0.58 mm.

Conclusions: This work introduces the use of multiple free-breathing CT scans for free-breathing ventilation measurements. The approach has some benefits over the traditional use

[e]Corresponding author: Daniel A Low, 200 Medical Plaza Way, Suite B265, Los Angeles, CA 90095, phone: (310)-562-2394, fax: (314)-362-8521, dlow@mednet.ucla.edu.

Disclosures:
The authors have no conflicts to disclose.

Data Availability: Data available on request from the authors

of 4DCT or breath-hold scans. The benefit over 4DCT is that FHFBCT does not have sorting artifacts. The benefits over breath-hold scans include the relatively small motion induced by quiet respiration versus deep-inspiration breath hold and the potential for characterizing dynamic breathing processes that disappear during breath hold.

Keywords

Computed-tomography based ventilation; fast helical free breathing computed tomography; 4DCT; 5DCT

I. INTRODUCTION

CT-based lung function imaging has traditionally been conducted using breath-hold. While breath-hold CT provides images without motion-induced or sorting artifacts, it suffers from the inability to be sensitive to dynamic processes and often involves images obtained at deep inhalation and exhalation, causing large deformations that are difficult to register. An alternative approach has been the use of 4DCT, which has been utilized with a series of challenges to extract ventilation information and is being employed for ventilation mapping in three clinical trials (NCT02528942, NCT02308709, NCT02843568)[1]. While 4DCT is used extensively for treatment planning when tumors are affected by breathing motion[2], 4DCT suffers from breathing sorting artifacts[3] and an inability to determine the accuracy of the relationship between the resulting images and the motion of the lung tissue which interfere with its use in quantitative lung dynamics analysis.

These breathing sorting artifacts present in 4DCT complicate and hinder functional measruements. Typically, deformable image registration is used to define a deformation vector field (DVF) that in turn can be used to calculate local tissue expansion and variations in Hounsfield Units (HUs) and thereby tissue density[4]. The local expansion, which has been considered a measurement of ventilation, is described using the DVF Jabobian[5]. Even small 4DCT sorting errors will cause relatively large errors in the calculation of the Jacobian and consequently the ventilation[6].

The fundamental reason that 4DCT has such sorting artifacts is the limited temporal sampling afforded by the conventional 4DCT approaches. 4DCT is acquired using either low-pitch helical acquisition or repeated cine acquisition, wherein in either case, the CT data for any region of the body are acquired over approximately 8 seconds, enough time to encompass between one and two breaths. The theory behind this is that as long as there are CT data for each breath, then CT scans can be reconstructed at any selected breathing phase. The limitation of this assumption is that of breathing regularity, which for many patients is insufficient to provide DVFs sufficiently artifact-free to provide artifact-free 4DCT image or support ventilation measurements.

Because of the limitations of 4DCT, our group selected repeated fast-helical free-breathing CT (FHFBCT) to provide the image data for radiation therapy treatment planning, which we term 5DCT[7]. FHFBCT is a shorthand for conventional helical CT that employ parameters such as gantry rotation speed and pitch that provide the maximum couch speed available from that CT scanner.[8] Repeated FHFBCT allows acquisition of image data at each couch

position spread out over many seconds to minutes, depending on the amount of time between successive scans, distributing the acquired image data over multiple breaths and improving the chances that the image data are acquired at a representative range of breathing depths and rates. 5DCT involves the generation of a breathing motion model that ties together the patient geometries measured by the set of FHFBCT scans and, but while the 5D motion model has been shown in general to be accurate to within approximately 3 mm[9], that accuracy is assumed to be insufficient for ventilation measurements.

Rather than assume a generalized breathing motion model, we use FHFBCT scans directly to measure breathing ventilation. The benefit of employing FHFBCT for this work is that the scans do not suffer from sorting artifacts, although they do exhibit limited motion blurring due to the finite scan times (defined here as the time required to scan a specific location, typically 0.23s-0.33s in our datasets). Our hypothesis is that the use of FHFBCT will enable highly accurate and precise DVF determinations, and subsequently, accurate and precise ventilation measurements. If this hypothesis is valid, it could enable significant advances in functional lung imaging.

II. MATERIALS AND METHODS

2.1 CT Acquisition and Synchronization

The CT scans were acquired repeatedly in alternating directions and with relatively low dose (first scan 160 mAs, subsequent scans 40 mAs)[10,11], and the first scan was used as the registration reference scan. Retrospective IRB approval was obtained for the 10 patient datasets used in this study. The total dose delivered by our scan protocol was approximately the same as commercial clinical 4DCT protocols. We used a 64-slice CT scanner (Siemens AS 64, Erlangen Germany), scanning the entire lungs using a pitch of 1.5, rotation time of 0.33s, and reconstructed with $0.977 \times 0.977 \times 1.000$ mm^3 voxels for 512×512 in-plane voxels. The patients were scanned 25 times in alternating directions with a 2 s pause between scans and an additional 15–30 s pause after the 15th scan due to a limitation in the scanner protocol sequencing software. A pneumatic bellows breathing surrogate was used to record the patient's breathing state[12]. Unlike the 5DCT protocol, only the breathing amplitude was needed, and not its rate. Simultaneous to the breathing surrogate, a CT-on signal was recorded from the CT scanner at a rate of 100 Hz. Both the internal bellows air pressure and the CT-on signal were recorded in real time using LABVIEW (National Instruments, Austin, TX).

Each CT scan DICOM file contained the CT slice acquisition time in the DICOM header. The CT on signal start and stop times were compared against the DICOM first and last slice acquisition time differences to evaluate if these time differences were consistent. The CT-on signal was longer than the difference between the first and last slice times due to the need to overscan and the CT warm-up time. The effective time of first slice acquisition was assumed to be half of the irradiation time, irradiation time being defined as the rotation period divided by the pitch, and the remaining difference was assumed to take place before the scan, with the assumption that the scanner beam would not operate after all projections were acquired. This provided an initial estimate of the synchronization between the DICOM time and the CT-on signal.

The bellows we employed had a known signal drift, likely caused by the air in the tube being heated by the patient. This drift needed to be measured and removed in order to provide a useful surrogate. The clinical 5DCT protocol used the skin surface in the CT scans as a stable drift-free metric, but for this application we elected to use the diaphragm dome to both remove the drift and fine-tune the CT synchronization time offset. Due to motion-induced blurring of the diaphragm, one of the CT images with minimal blurring was selected as the reference for this process (the drift-correction reference scan). A point near the diaphragm dome was manually selected on the drift-correction reference scan. This point was used as the center of a 45 × 45 voxel column and the diaphragm within each column was crudely aligned using rigid registration (MATLAB, Mathworks, Natick MA). CT scan profiles through a subsequent 11 × 11 array of voxel columns, oriented craniocaudally and centered on the selected voxel were extracted and blurred using a 6 mm standard deviation one-dimensional Gaussian kernel. The blurring allowed the CT Hounsfield profiles in scans with and without motion blurring to be subsequently fit to error functions. The error function fit residuals were calculated and profiles with the largest residuals were observed to intersect vessels or other structures within the parenchymal tissues, so in order to remove these profiles from subsequent analysis, only profiles with root-mean square residual HUs of less than 50HU were retained. The mean differences between the drift-correction reference scan and other scans' error function inflection points were used as the relative diaphragm shift measurement.

The full images were larger than the lungs, so the images were manually cropped in the lateral and anteroposterior directions to include all of the lungs. All CT slices were retained to simplify subsequent time synchronization. Breathing motion induces image blurring that for many applications is not significant, but for purposes of this registration was too large to ignore. Therefore, we selected superior regions of the lungs that had minimal blurring. We selected rectilinear regions of interest (ROIs) and because of patient-to-patient differences in the lung shapes, the ROIs varied in size.

2.2 Image registration

2.2.1 Initial using pTV—The image registration process was divided into two steps. The initial step employed a published registration algorithm, allowing us to take advantage of sophisticated and well established registration approaches. For this purpose, we selected the pTV registration approach[13]. In their approach, isotropic Total Variation (TV) regularization was used to enable accurate registration near lung-chest wall interfaces. They also developed the TV-regularization for parametric displacement fields and provided an efficient numerical solution scheme using the Alternating Directions Method of Multipliers. They had shown that their approach, when applied to published 4DCT datasets of 10 patients[14,15], exhibited a mean 3D registration error of 1.0 mm out of an average motion of 8.52 mm. In this work the subsequent registration result was termed the pTV registration. The pTV code was downloaded from (https://github.com/visva89/pTVreg) and the non-default parameters are shown in Table 1.

2.2.2 Secondary Registration—Because the ventilation calculation would rely on the DVF Jacobians, which were determined from the DVF gradients, we were concerned

that the pTV registration might yield complex DVF gradients that would yield unphysical Jacobians and our subsequent registration would need to replace those gradients. To avoid this while also allowing the pTV to be used as an initial registration, we sampled the pTV registration on a 10 × 10 × 10 voxel (9.77 × 9.77 × 10 mm^3) grid and linearly interpolated the registration vector fields in between. The full pTV registration results were also used to evaluate the ventilation and other quantities for comparison against the two-step approach.

Objective Function: Similar to other registration approaches, the secondary registration employed an objective function with multiple terms, with each term intended to assert a physical principle. Because the CT scans were acquired during free breathing, they were assumed to differ only due to the breathing state, which explicitely assumed that there was no variation due to the cardiac cycle or non-periodic changes. In order to avoid the impact of motion-induced blurring, the registration analysis was restricted to the upper portions of the lungs. The lung tissue density was assumed to be measurable using the CT Hounsfield Units by scaling the linear attenuation coefficient to the physical density. As part of the CT protocol, the CT scanner HU calibration had been checked before each patient was scanned such that the CT values for air and water were −1024 and 0, respectively.

The first objective function term was intended to localize high contrast objects such as blood vessels. If the lung tissue density did not change between scans, the objective function term would simply be the difference between the reference and target HU values. In order to compensate for the local ventilation-induced variation in parenchymal HU values, the voxel-specific HU term was modified in a method similar to Gorbunova et al[16], by using what we term ventilation-corrected HUs:

$$HU'_i \equiv HU_i + \frac{dHU}{dA}(A_R - A_i) \tag{1}$$

where the ventilation-corrected HU'_i was computed from the raw deformed HU_i for image i relative to the reference image R, A_i and A_R were the corrected bellows-determined amplitudes for images i and R, respectively. $\frac{dHU}{dA}$ was the least-squares slopes of the raw deformed HU values for all 25 scans as functions of their respective corrected bellows-determined amplitudes. This process provided an estimate of the variation in HUs with respect to breathing amplitude that, because of the large number of scans, was relatively insensitive to voxel-to-voxel noise.

The first objective function term for image i (at each voxel) relative to the reference image R was then:

$$\Delta HU^i = HU'_i - HU_R \tag{2}$$

While $\Delta HU'_i$ was most useful in registering steep image gradient regions, such as vessel boundaries, it would not be as useful in registering parenchymal tissues because of the lack of contrasting objects. The second objective function term was based on mass conservation and compared the image Jacobian and the local tissue density ratio[6].

Figure 1 graphically illustrates the relationship between the DVF Jacobian and the tissue density ratio of a voxel represented in images *i* and *R*. For this voxel, the Jacobian/tissue density ratio location on the graph was defined as Γ. The DVF compliance with mass conservation was characterized as the Euclidian distance between the point Γ and the line corresponding to $J_{iR} = \rho_R/\rho_i$. That distance was termed ΔΓ

$$\Delta\Gamma_i \equiv \frac{J_{iR} - \rho_R/\rho_i}{\sqrt{2}} \tag{3}$$

and was used as the second objective function term. This term served to guide the registration such that the DVF Jacobians reflected the measured density differences between the two images. Since the HU noise was relatively large (standard deviation of 30HU), for low density tissues the denominator ρ_i could get quite small for some voxels, leading to a few voxels with very large values of ΔΓ. This was managed by the fact that in addition to mass conservation being reflected using $J_{iR} = \rho_R/\rho_i$, it could also be reflected using $\frac{1}{J_{iR}} = \rho_i/\rho_R$ or $\Delta\Gamma_i' \equiv \frac{1/J_{iR} - \rho_i/\rho_R}{\sqrt{2}}$ so ΔΓ was used when $\rho_i > \rho_R$ and $\Delta\Gamma_i'$ when $\rho_i \leq \rho_R$. To provide a smooth transition across $\rho_R = \rho_i$, a linear admixture of $\Delta\Gamma_i$ and $\Delta\Gamma_i'$ was used when the ratio was between 1.1 and 1/1.1.

A useful feature of the ΔΓ objective function term was its natural DVF regularization. Without regularization, the ΔHU term would in principle allow unphysical deformations as long as it minimized the HU differences, but the use of the DVF Jacobian in the ΔΓ term served to regularize the DVF behavior.

We elected to use no additional explicit regularization term and emphasize the physical constraints. Our hypothesis was that the initial DVF provided by pTV would provide a registration that was sufficiently close to allow the ΔHU^i and $\Delta\Gamma_i$ terms to improve registration accuracy. We elected to use the L_1 norms of the objective function terms. The comprehensive objective function was therefore

$$\sum_i \left|\Delta HU_i^i\right| + \omega\left|\Delta\Gamma_i\right| \tag{4}$$

where ω was a user-selected weighting factor.

Rectilinear Control Point Grid: To test the ventilation measurement using FHFBCT, a rectangular region of interest (ROI) was selected from the right upper lung of the 10 patients. Table 1 summarizes the ten ROIs used in this study.

pTV provided 24 sets of 3-dimensional DVF values at each reference voxel. The pTV registration DVFs were sampled at 10 × 10 × 10 voxel spacing and these locations defined as the first set of control points. Because these initial control points lay in a rectilinear grid, simple trilinear interpolation was used to generate the full DVFs when needed. For this first pass, ω = 0.5 and the registration was allowed to undergo 20 iterations.

DVF and Control Points: While a lot of attention is placed on the objective function, the method of defining the DVF itself is also critical to a physically accurate registration. There are a number of methods to describe DVF vector fields, including thin-plate splines, optical flow, B-splines, and Demons. As mentioned above, linear interpolation was used to define the DVF between control points. This allowed the ventilation to change abruptly at parenchyma-soft-tissue boundaries, which included vessels, large bronchi, and the chest wall. Selection of control points was based on the concept that the ventilation needed to be able to change across such high contrast regions and selection was therefore based on the local image gradient. Starting with the original 10 × 10 × 10 voxel control point array, 4mm diameter spherical masks were placed surrounding each control point and the masks used to exlude adding control points within those masked regions. Within the remaining ROI, the point in the unmasked reference image with the steepest gradient was selected as the next control point and a 4 mm diameter spherical mask was placed around it. This process of control point selection repeated until no volume remained within the ROI. The benefits of this approach included physically spacing control points so that they didn't cluster and allowing positioning of control points throughout a range of gradients to enable selection of both large and small vessels and various structures.

Registration Workflow: The registration results from the initial cubic control point registration were linearly interpolated to the control point locations and the registration restarted from that point, this time using both the initial and gradient-based control points. The objective function was the same, with the $\Delta\Gamma$ weighting factor ω=3. The registration was allowed to undergo 15 iterations. Subsequent DVF interpolations were conducted by creating a Delaunay mesh and using tetrahedral interpolation.

2.3 Ventilation

Two methods have been used to determine ventilation from CT scans[17]; using the HU values, converting to density and computing the density difference or ratio[4,18–20], or using the DVF Jacobian[5,6]. Due to the relatively large noise in the HU values, we elected to use the Jacobian method. Also, since there were 25 images, ventilation was defined based on the collective behavior of the Jacobian with respect to the breathing amplitude. For this work, the Jacobian was assumed to change linearly with respect to the breathing amplitude and was independent of breathing rate. The ventilation V was defined as the the slope of a linear fit to the Jacobian with respect to the breathing amplitude. This analysis was conducted on a voxel-by-voxel basis.

$$V \equiv \frac{dJ}{dA} \tag{5}$$

This approach defaults to the conventional 4DCT definition of Ventilation if there are only two images, one at inhalation and one at exhalation, and if the 4D definition of amplitude is employed (as opposed to the percentile definition used in our approach). Ventilation for 4DCT is often defined as $V = J - 1$,[21] which results in the same value as our approach if equation 5 is used for only inhalation and exhalation and the amplitude difference is normalized to 1.

2.4 Registration Evaluation

As described earlier, the change in Jacobian, and consequently ventilation, is very sensitive to the DVF vector field. Therefore, using a landmark-based registration evaluation approach would be insufficient to determine the accuracy of the secondary ventilation measurement approach. Given that there was no independent ground truth for these images, the quantity $\Delta\Gamma$ was used to evaluate the ventilation for the initial and secondary registrations. As shown in Equation 3, $\Delta\Gamma$ is a function of the ratio of HU-calculated densities, which due to the HU noise as identified earlier, could lead to spuriously large values of $\Delta\Gamma$. In this case, since the goal was to determine ventilation over a distance scale of a few millimeters, $\Delta\Gamma$ distributions were calculated using blurred density distributions, blurring the the density distribution using a 3-dimensional Gaussian with a radial standard deviation (1.2 mm) such that 92% of the total weighting included voxels were within 3 mm of the nominal voxel location.

III. RESULTS

Table 2 shows a summary of the volumes and numbers of control points used for each patient. The table also shows a measure of breathing irregularity. There are no established and accepted definitions of breathing irregularity, so a simple method for describing these irregularities was developed. The amplitudes were normalized by the 10^{th} and 90^{th} percentile amplitudes (10^{th} percentile = 0, 90^{th} percentile = 1), selected arbitrarily to span the range of breathing while avoiding outliers. The peak inhalation and exhalation times were detected using an amplitude thresholding method, and the amplitude differences between the successive inhalations and exhalations were determined. These amplitude differences formed a distribution and the amplitude irregularity was defined as the difference between the 10^{th} and 90^{th} percentile of these values. A value of 0 would mean that there was no variation in breath-to-breath inhalation to exhalation amplitude differences. As shown in the table, the smallest and largest values were 0.18 and 0.69, respectively, a factor of almost 4, and an amplitude irregularity indicated that from the least to most varying amplitude differences (the 10^{th} to 90^{th} percentiles) varied by almost 70%. The minimum to maximum variation was greater, but we felt that defining irregularity by the extreme breaths would be misleading.

Figure 2a shows an example of the relationship between the drift and time corrected bellows signal and the corresponding relative diaphragm shifts used as the breathing amplitude for patient 111. The line shows the quadratic curve used to convert subsequent corrected bellows signals to diaphragm positions for use as the patient's breathing amplitude. Figure 2b shows the fit residuals as functions of the time offset and drift correction for the same patient. The minimum residual was used to determine the optimal drift and time offset values. The amplitude measurement error, defined as the root-mean squared residual divided by the 90^{th} percentile bellows amplitude range, was 3.3% for this patient. Table 3 shows a summary of the diaphragm position residual for each of the patients. The mean value was 5.2%+/−1.7% for all 10 patients. Statistically, the diaphragm position errors were uncorrelated to the amplitude irregularities (correlation coefficient 0.22, p value 0.53).

Figure 3 shows examples of the reference images and averaged images for patients 103, 107, and 111. The averaged images were generated by averaging the ventilation-adjusted HUs (calculated using equation 1).

Figure 4 shows examples of the Jacobians from three voxels of patient 111 generated using the secondary registration versus their corresponding breathing amplitude. Shown are one voxel in the chest wall (Figure 4a) and two parenchymal voxels. The values of the Jacobian are essentially 1.0 for the voxel in the chest wall, and the Jacobian ranges from approximately 1 to 1.2 and from 1 to 1.4 at the other two voxels. For these examples, the amplitude is shown as percentages of the 10^{th} to 90^{th} percentile amplitude range. The Ventilation was calculated using a linear fit and Equation 5. The resulting ventilation values were 0.01, 0.23 and 0.48.

Figure 5 shows examples of the ventilation distribution for sagittal slices through three of the patient's datasets. Patient 103 (Figure 5a) exhibited the largest ventilation values of the 10 patients, with voxels exhibiting ventilation values of up to 1, which would correspond to doubling of the voxel volume. Patient 107 (Figure 5b) shows a relatively homogeneous ventilation, while the ventilation pattern for patient 111 (Figure 5c) is relatively heterogeneous. The same slices are shown for the initial pTV registration (Figures 5d, 5e, and 5f), exhibiting ventilation distributions with similar levels of heterogeneity, but with different patterns. In order to determine if there was an overall bias between the two registration approaches, the mean ventilation differences were computed and the differences are shown in Table 4. All of the mean ventilation differences were small, with only patient 105 having an average magnitude difference greater than 0.02.

Table 4 also shows the standard deviation of the ventilation difference of the 10 patients. The standard deviations show that while the mean ventilations were almost zero, the voxel-to-voxel differences between the two registrations yielded ventilations that differed by approximately 0.1.

Figure 6 shows examples of $\Delta\Gamma$ distributions for the patient ventilations shown in Figure 5 and at the same positions. There is a clear difference between the overall $\Delta\Gamma$ distributions, especially in magnitude. While the $\Delta\Gamma$ values decrease once the secondary registration is used, the values do not universally decrease to small values. In general, there are always small regions of relatively large values of $\Delta\Gamma$ (defined here as >0.2), and the regions in the secondary registration that exhibit large values are at common locations with regions that have large values in the pTV registration. Table 4 shows the 90^{th} percentile values of $\Delta\Gamma$ for both registrations for voxels in the lungs, as well as their ratio, showing that according to this metric, the registration improved $\Delta\Gamma$ by a factor of 1.86+/−0.38. The differences between the DVFs of the two registrations are shown for the 3 presented cases in Figure 7. The vast majority of changes in DVF vectors were sub-millimeter, highlighting the sensitivity of the Jacobian and consequently the ventilation, on the DVF results. Table 4 also lists the 90^{th} percentile DVF differences, with a mean value across all patients of only 0.58mm +/− 0.24mm.

IV. DISCUSSION

We presented a preliminary investigation of using multiple FHFBCT scans for ventilation mapping. The structure of the investigation included using a published registration technique, pTV for the initial registration, followed by a second registration using an objective function that employs ventilation-corrected HU and conservation of mass (ΔΓ).

There are a number of benefits of using FHFBCT as the CT acquisition protocol. First, it does not exhibit the breathing sorting artifacts inherent in 4DCT, and should therefore be useable for patients with irregular breathing patterns. Of the 10 patients selected for this study, 3 showed large breathing irregularities that would likely have resulted in substantial 4DCT sorting artifacts. Second, the collective behavior of the 25 scans could be used to characterize ventilation. In the first case, the ventilation-correction process used a linear fit between the HUs and breathing amplitude to reduce the ventilation-induced differences between the CT scans to improve the localization of common vessels and other structures. In the second case, the 25 Jacobian values were used to measure the ventilation. In both of these circumstances, the consequence of errors of specific registration pairs would only minimally affect the results and significant outliers could in principle be detected, although this approach was not employed here. Third, unlike ventilation measurements that use deep inspiration and expiration scans, the deformation between the FHFBCT scans are relatively small, improving the overall registration and subsequently ventilation accuracy.

One of the limitations of this work is that the evaluation metric ΔΓ was also one of the terms in the secondary registration objective function, so a reduction in ΔΓ was effectively guaranteed. However, given that ΔΓ is a measurement of mass conservation, we feel that it remains appropriate to use for the evaluation of the registration results. Still, an independent registration verification method should be developed that has the sensitivity needed to validate registration to the level needed for use in ventilation characterization.

Another limitation in this study was ignoring the cardiac cycle in the registration analysis. Previous studies have shown that the lung blood pool changes approximately 50 ml over the cardiac cycle[22], which would change parenchymal HU values and possibly the diameters of blood vessels. Ignoring these effects would likely appear as uncorrelated noise or errors in the registration process, and may degrade the ventilation accuracy. In the future, we will add ECG measurements to the FHFBCT acquisition protocol to allow an analysis of registration fluctuation as a function of the cardiac cycle.

The FHFBCT scan protocol employed is designed for our clinical 5DCT program and has not been optimized for ventilation measurements. One consequence of this is the relatively large dose delivered by the FHFBCT protocol which while similar to that delivered by commercial 4DCT protocols, would preclude its use as a common diagnostic study. A prospective scanning protocol that employed fewer scans but at optimized breathing phases, would allow the use of fewer scans and consequently lower dose.

The reason for analyzing the superior portion of the lungs was to avoid the lung regions with larger motion-induced blurring. The scanner we employed was relatively fast, with the image data acquired within approximately 0.33s. However given that lung tissues can

move approximately 1 cm s^{-1} during mid-inspiration and mid-expiration, motion-induced blurring for these tissues would be multiple voxels and the consequential motion-induced blurring could impact the secondary registration results. Even fast single-source scanners cannot image faster than approximately 100ms, so motion-induced blurring could still exist at the single voxel level. Our group recently developed a method for reducing breathing-induced blurring in lung CT scans and has applied for a patent. Work is ongoing to show the reduction in blurring provided by that approach and we expect that with the blurring removed, the proposed registration and analysis methods will be applicable to the entire lungs.

One of the most preliminary aspects of this study was the generation of the control points. The placement of the control points governs the registration's ability to adjust the registration Jacobian to model variations in ventilation. This is especially important at soft-tissue to parenchymal tissue boundaries, which essentially include all blood vessel and larger bronchial surfaces. Just placing individual control points along these surfaces would be impractical and the corresponding DVF ill-posed, so an improved approach to managing the DVF along these surfaces needs to be developed to allow for physically realistic DVFs while maintaining reasonable registration calculation speeds.

The term $\Delta\Gamma$ includes a ratio of the CT-measured densities, which means that it is undefined for air pockets such as the trachea, large bronchi, and air-filled bullae. These regions were avoided in this preliminary work by the ROI selection process. Small airways did exist within some scans, but they were of sufficiently small diameter that partial-volume effects maintained their densities at non-zero values. While DVFs are defined for air cavity boundaries, they are undefined in the cavities themselves, so a detection and masking process might be needed to manage them.

The secondary registration approach relied heavily on the CT-calculation of density. The accuracy and stability of this relationship is aided by routine quality assurance of the CT scanner using HU calibration phantoms because the CT scanner is used for radiation therapy treatment planning. Residual CT value errors will still occur due to streaking artifacts from high density objects, uncompensated beam hardening, and out-of-field artifacts. The impact of these artifacts on the registration needs to be investigated, but since $\Delta\Gamma$ employs only the ratio of the densities, it minimizes to first order the sensitivity of $\Delta\Gamma$ to such artifacts.

One of the most exciting aspects of this work is the potential for measuring high spatial resolution dynamic ventilation processes. Because we acquire the CT data during respiration, we might be able to detect air trapping or bronchial collapse, with associated diagnostic value to pulmonologists or radiologists. Similar work has been proposed by Shao et al[23] using 4DCT and coached breathing. Our proposed free-breathing process will generate dynamic data that would be the first of its kind and will require further detailed analysis of the registration results.

V. CONCLUSIONS

The use of multiple FHFBCT scans for ventilation measurements has been introduced as well as the use of collective ventilation correction for HU comparisons and the use of ΔΓ in both the registration objective function and for evaluating the registration accuracy.

Some significant challenges remain. We did not consider cardiac-induced motion, which would appear in this study as uncorrelated changes in the local Jacobian unrelated to local tissue density change. The development of control-point selection and registration verification remain two important research directions. Finally, prospective CT scanning could significantly reduce the radiation dose, opening up this approach for diagnostic purposes.

Acknowledgments:

This work was supported in part by TRDRP and NIH R56 HL139767–01. The first author's daughter belonged to the sorority ΔΓ during college (Case Western Reserve) and they provided her with great opportunities to engage in social action and social justice with other terrific women, so to express our appreciation we employed the Greek letter Γ to represent a voxel's location in the Jacobian versus density ratio space and ΔΓ to represent the relative non-compliance with mass conservation.

References

1. Kipritidis J, Tahir BA, Cazoulat G, et al. The VAMPIRE challenge: A multi-institutional validation study of CT ventilation imaging [published online ahead of print 2018/12/24]. Med Phys 2019;46(3):1198–1217. [PubMed: 30575051]
2. De Oliveira Duarte S, Rancoule C, He MY, et al. Use of 4D-CT for radiotherapy planning and reality in France: Data from a national survey [published online ahead of print 2019/07/25]. Cancer Radiother 2019;23(5):395–400. [PubMed: 31331842]
3. Watkins WT, Li R, Lewis J, et al. Patient-specific motion artifacts in 4DCT [published online ahead of print 2010/07/17]. Med Phys 2010;37(6):2855–2861. [PubMed: 20632597]
4. Simon BA. Non-invasive imaging of regional lung function using x-ray computed tomography [published online ahead of print 2003/02/13]. J Clin Monit Comput 2000;16(5–6):433–442. [PubMed: 12580227]
5. Castillo E, Castillo R, Vinogradskiy Y, et al. Robust CT ventilation from the integral formulation of the Jacobian [published online ahead of print 2019/02/20]. Med Phys 2019;46(5):2115–2125. [PubMed: 30779353]
6. Reinhardt JM, Ding K, Cao K, Christensen GE, Hoffman EA, Bodas SV. Registration-based estimates of local lung tissue expansion compared to xenon CT measures of specific ventilation [published online ahead of print 2008/05/27]. Med Image Anal 2008;12(6):752–763. [PubMed: 18501665]
7. O'Connell D, Thomas DH, Lewis JH, et al. Safety-oriented design of in-house software for new techniques: A case study using a model-based 4DCT protocol [published online ahead of print 2019/01/19]. Med Phys 2019;46(4):1523–1532. [PubMed: 30656699]
8. Thomas DH, Tan J, Neylon J, et al. Investigating the minimum scan parameters required to generate free-breathing motion artefact-free fast-helical CT [published online ahead of print 2017/11/04]. Br J Radiol 2018;91(1082):20170597. [PubMed: 29099616]
9. Dou TH, Thomas DH, O'Connell DP, Lamb JM, Lee P, Low DA. A Method for Assessing Ground-Truth Accuracy of the 5DCT Technique [published online ahead of print 2015/11/05]. Int J Radiat Oncol Biol Phys 2015;93(4):925–933. [PubMed: 26530763]
10. Low DA, Parikh PJ, Lu W, et al. Novel breathing motion model for radiotherapy [published online ahead of print 2005/09/06]. Int J Radiat Oncol Biol Phys 2005;63(3):921–929. [PubMed: 16140468]

11. Low DA, White BM, Lee PP, et al. A novel CT acquisition and analysis technique for breathing motion modeling [published online ahead of print 2013/05/04]. Phys Med Biol 2013;58(11):L31–36. [PubMed: 23640212]
12. Lu W, Low DA, Parikh PJ, et al. Comparison of spirometry and abdominal height as four-dimensional computed tomography metrics in lung [published online ahead of print 2005/08/27]. Med Phys 2005;32(7):2351–2357.
13. Vishnevskiy V, Gass T, Szekely G, Tanner C, Goksel O. Isotropic Total Variation Regularization of Displacements in Parametric Image Registration [published online ahead of print 2016/09/23]. IEEE Trans Med Imaging 2017;36(2):385–395. [PubMed: 27654322]
14. Castillo E, Castillo R, Martinez J, Shenoy M, Guerrero T. Four-dimensional deformable image registration using trajectory modeling [published online ahead of print 2009/12/17]. Phys Med Biol 2010;55(1):305–327. [PubMed: 20009196]
15. Castillo R, Castillo E, Guerra R, et al. A framework for evaluation of deformable image registration spatial accuracy using large landmark point sets [published online ahead of print 2009/03/07]. Phys Med Biol 2009;54(7):1849–1870. [PubMed: 19265208]
16. Gorbunova V, Sporring J, Lo P, et al. Mass preserving image registration for lung CT [published online ahead of print 2012/02/18]. Med Image Anal 2012;16(4):786–795. [PubMed: 22336692]
17. Vinogradskiy Y. CT-based ventilation imaging in radiation oncology [published online ahead of print 2019/04/05]. BJR Open 2019;1(1):20180035. [PubMed: 33178925]
18. Yamamoto T, Kabus S, von Berg J, et al. Reproducibility of four-dimensional computed tomography-based lung ventilation imaging [published online ahead of print 2012/09/15]. Acad Radiol 2012;19(12):1554–1565. [PubMed: 22975070]
19. Guerrero T, Sanders K, Castillo E, et al. Dynamic ventilation imaging from four-dimensional computed tomography [published online ahead of print 2006/02/10]. Phys Med Biol 2006;51(4):777–791. [PubMed: 16467578]
20. Guerrero T, Sanders K, Noyola-Martinez J, et al. Quantification of regional ventilation from treatment planning CT [published online ahead of print 2005/06/07]. Int J Radiat Oncol Biol Phys 2005;62(3):630–634. [PubMed: 15936537]
21. Ding K, Cao K, Fuld MK, et al. Comparison of image registration based measures of regional lung ventilation from dynamic spiral CT with Xe-CT [published online ahead of print 2012/08/17]. Med Phys 2012;39(8):5084–5098. [PubMed: 22894434]
22. Ugander M, Jense E, Arheden H. Pulmonary intravascular blood volume changes through the cardiac cycle in healthy volunteers studied by cardiovascular magnetic resonance measurements of arterial and venous flow [published online ahead of print 2009/11/03]. J Cardiovasc Magn Reson 2009;11:42. [PubMed: 19878570]
23. Shao W, Patton TJ, Gerard SE, et al. N-Phase Local Expansion Ratio for Characterizing Out-of-Phase Lung Ventilation [published online ahead of print 2020/01/04]. IEEE Trans Med Imaging 2020;39(6):2025–2034. [PubMed: 31899418]

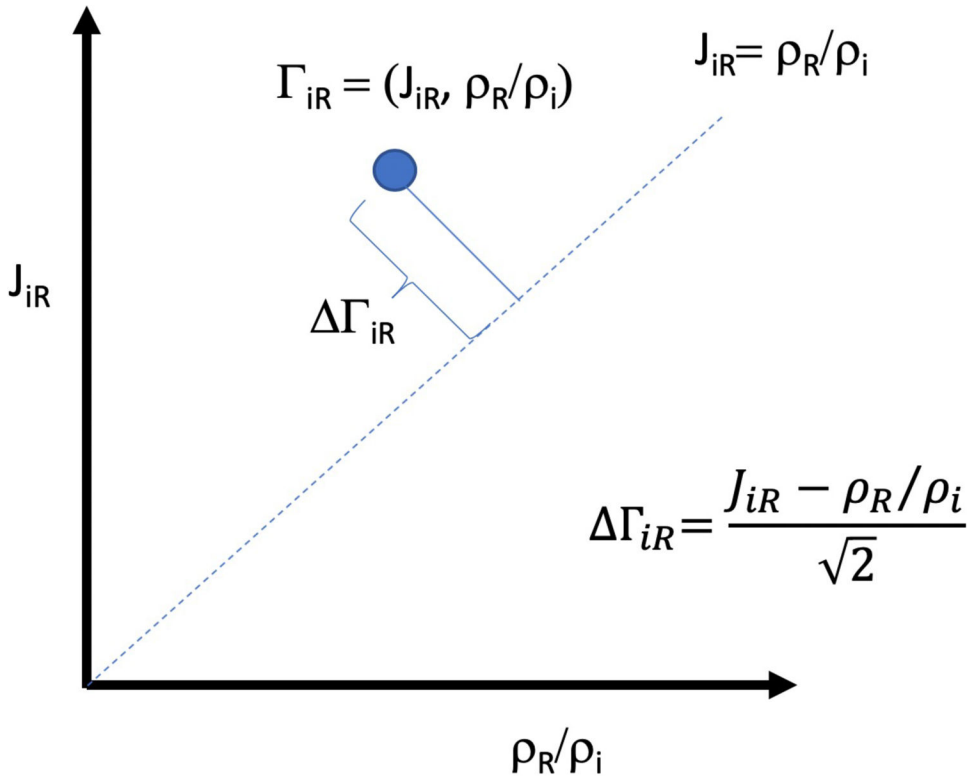

Figure 1:
Graphical representation of the conservation-of-mass error assessment ΔΓ.

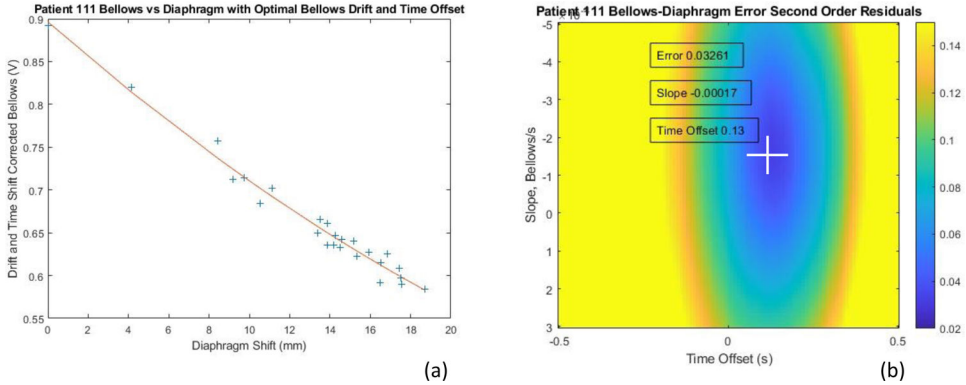

Figure 2.

a) Relationship between the drift-corrected and time-shift corrected bellows and the measured diaphragm shift. b) Residuals of bellows 2nd order fit as a function of the bellows drift and time offset, including the optimal value of 0.13s time offset and a slope of −0.00017 inHg/s. The corresponding error, 3.3%, is defined as the root-mean squared residual values divided by the 10th to 90th percentile bellows signal during the CT acquisition session.

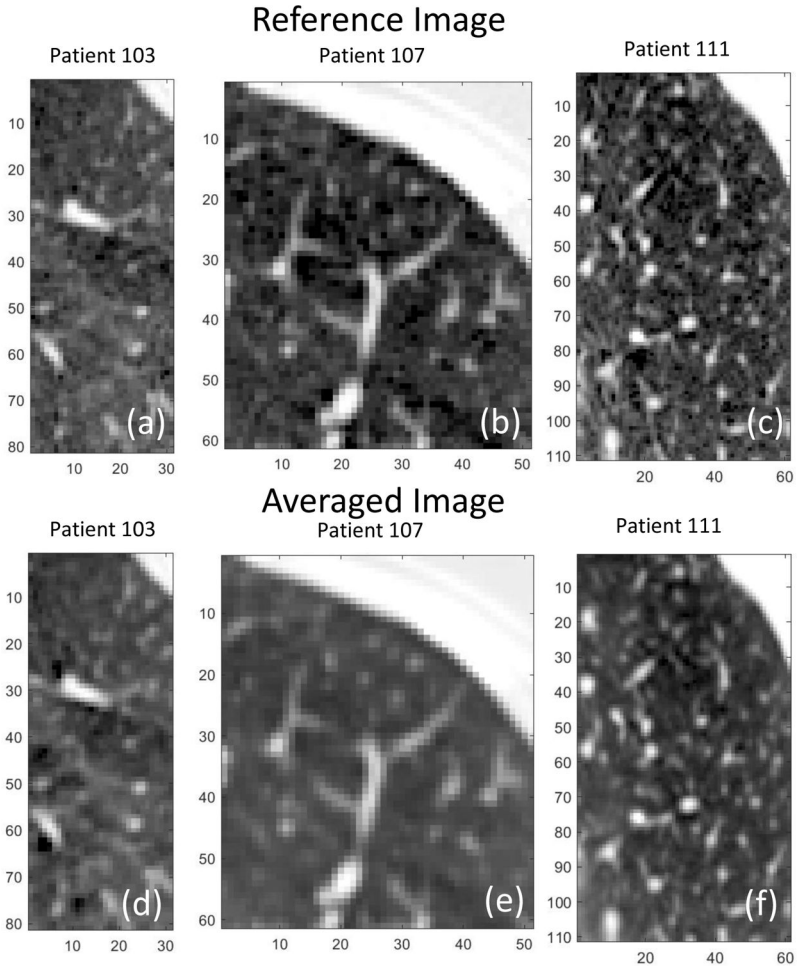

Figure 3:

Reference and averaged images (ventilation-corrected to reference amplitudes) for three sample patients. (a)-(c) Reference images. (d)-(f) Corresponding averaged images.

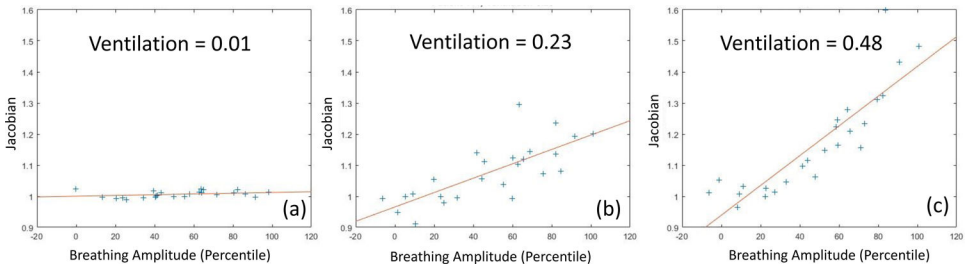

Figure 4:

Examples of single-voxel Jacobian values and corresponding fits that define the ventilation for three voxels of patient 111. (a) Voxel in the chest wall. (b) and (c) Voxels in the parenchyma.

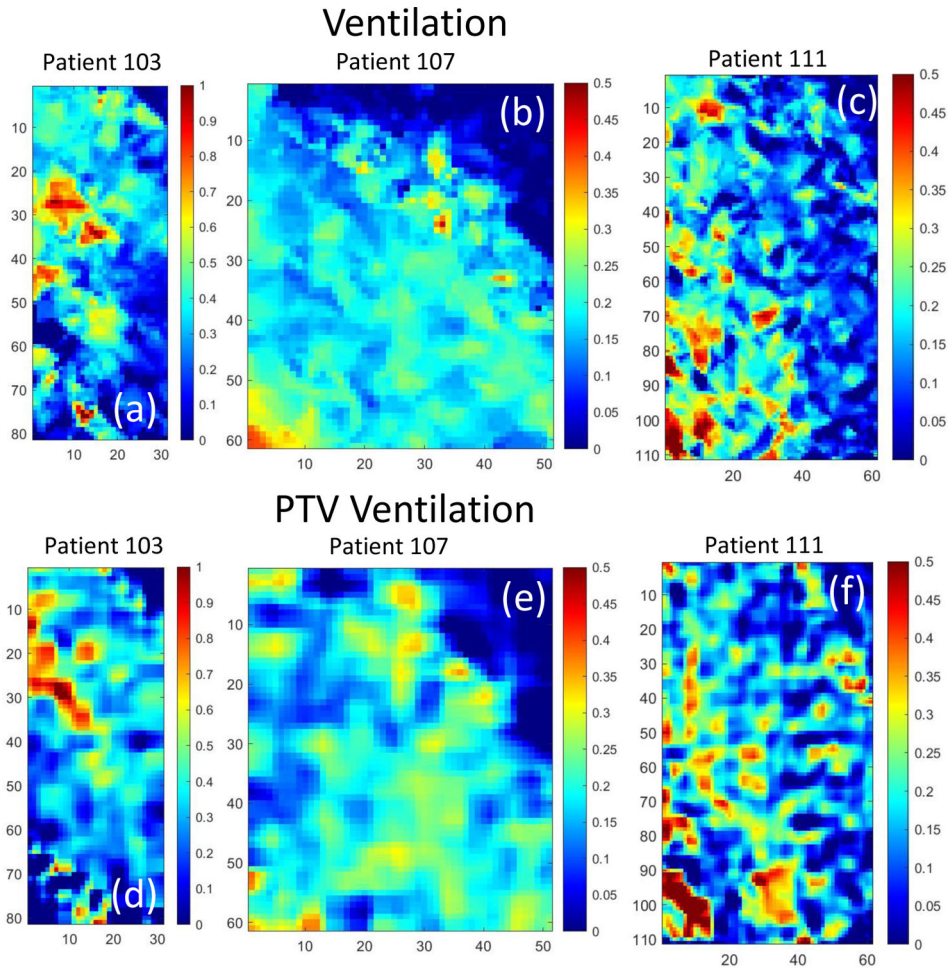

Figure 5:

Comparison of Ventilation maps for three representative patients. (a) – (c) The secondary registration. (d)-(f) pTV registration.

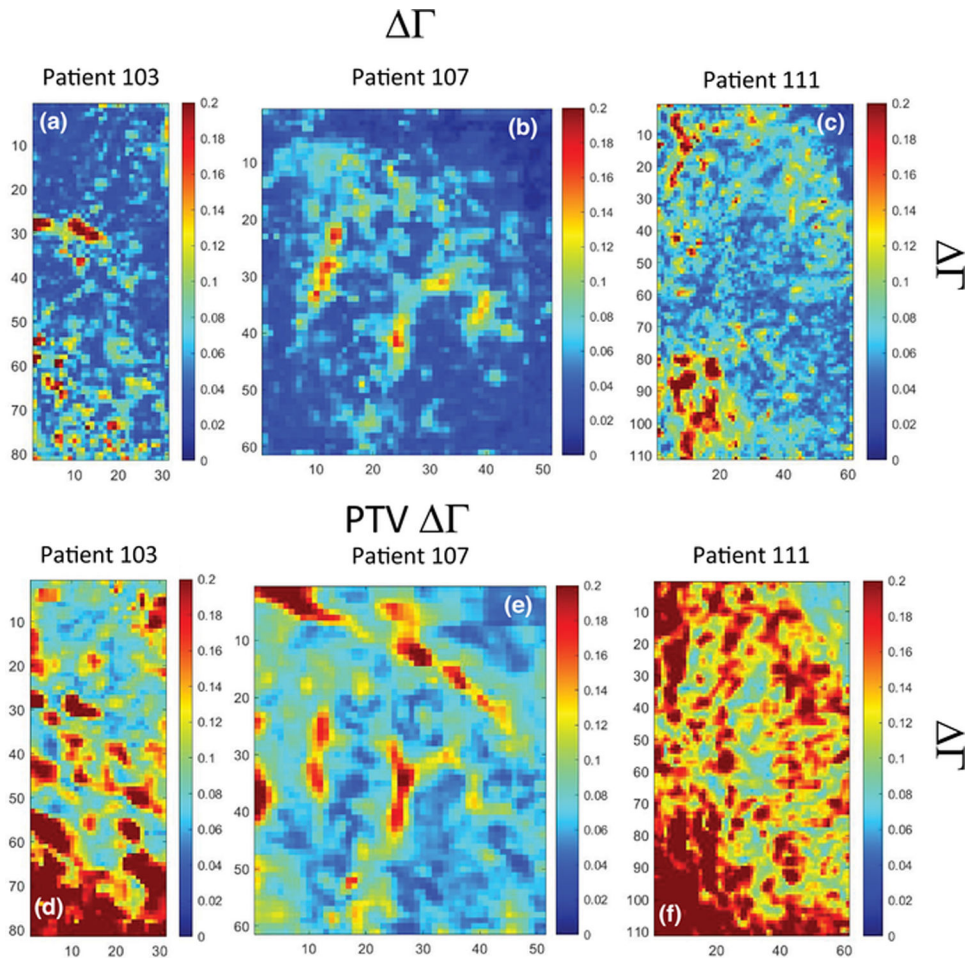

Figure 6:

Sagittal slices of ΔΓ from the same 3 patients shown in Figure 3. (a) to (c) secondary registration, (d) to (f) initial pTV registration.

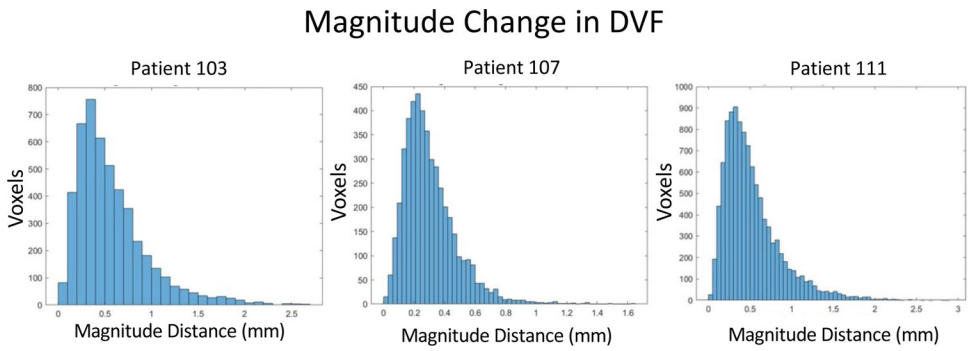

Figure 7:

Histograms of change in DVF vectors between initial pTV and secondary registrations for tissues within the lung for three of the studied patients.

Table 1.

Non-default parameter settings for pTV registration used as initial deformable image registration.

Parameter Label	Parameter Value
opts.loc_cc_approximate	false
opts.pix_resolution	[1 1 1]
opts.display	‘off’
opts.k_down	0.7
opts.interp_type	0
opts.metric	‘loc_cc_fftn’
opts.metric_param	[1,1,1] * 2.1
opts.scale_metric_param	true
opts.isoTV	0.11
opts.csqrt	5e-3
opts.spline_order	1
opts.border_mask	5

Table 2.

Characteristics of patient region-of-interest volumes used for registration and evaluation and the breathing amplitude irregularity.

Patient Number	Volume (voxels)	Volume (cc)	Number of Control Points	Amplitude Irregularity
101	51×71×51	176	2283	0.43
103	51×81×31	122	1618	0.69
105	31×71×51	107	1419	0.68
106	61×71×71	293	3720	0.18
107	61×51×51	181	2316	0.41
108	51×111×51	275	3488	0.41
109	51×71×61	211	2687	0.30
110	51×91×41	181	2337	0.59
111	51×111×61	329	4122	0.51
112	41×61×41	98	1298	0.52

Table 3:

Residual bellows to diaphragm position fit after linear drift and time offset corrections were applied to the bellows signal. The diaphragm position error is defined as the root-mean squared residual values divided by the 10^{th} to 90^{th} percentile bellows signal during the CT acquisition session

Patient Number	Diaphragm Position Error
101	4.5%
103	3.8%
105	6.5%
106	2.8%
107	5.4%
108	5.8%
109	7.2%
110	8.0%
111	3.3%
112	5.0%
Average	5.2%+/−1.7%

Table 4

Voxel-to-voxel average difference +/− root-mean square differences of the ventilation as calculated by the initial pTV and secondary registration approaches. 90th percentile DVF change between the PTVreg and secondary registrations, showing the relatively small added deformations. The mean values of ΔΓ for both the secondary and PTVreg registrations as well as the ΔΓ ratios. In all cases the values of ΔΓ were reduced by almost 50%.

Patient	RMS Ventilation Difference	90th percentile DVF Change (mm)	Secondary Registration 90th Percentile ΔΓ	PTVreg 90th Percentile ΔΓ	Ratio ΔΓs
101	−0.003+/−0.065	0.50	0.067	0.111	1.66
103	0.002+/−0.279	1.06	0.110	0.295	2.69
105	−0.023+/−0.102	0.49	0.064	0.139	2.19
106	−0.008+/−0.100	0.42	0.068	0.118	1.73
107	−0.004+/−0.095	0.53	0.076	0.123	1.62
108	−0.004+/−0.088	0.50	0.090	0.147	1.64
109	0.004+/−0.060	0.43	0.068	0.115	1.70
110	−0.005+/−0.053	0.40	0.061	0.095	1.54
111	−0.009+/−0.145	0.97	0.125	0.279	2.24
112	−0.019+/−0.074	0.46	0.065	0.106	1.63
Average	−0.007+/−0.009	0.58 +/− 0.24	0.079+/−0.022	0.153+/−0.072	1.86+/−0.38